Silicon quantum dots in microdisk resonators: Whispering-gallery modes, stress-induced Q-factor tuning and enhancement

G. Pucker[a*], M. Ghulinyan[a], A. Pitanti[b], M. Xie[b], D. Navarro-Urrios[b‡], A. Lui[c], L. Pavesi[b], and A. Simoni[a]
[a] Advanced Photonics & Photovoltaics, Fondazione Bruno Kessler, I-38050 Trento, Italy;
[b] Nanoscience Lab., Dept. Physics, University of Trento, I-38050 Trento, Italy;
[c] M2B2, Fondazione Bruno Kessler, I-38050 Trento, Italy

ABSTRACT

We report on visible light emission from Si quantum dot (QD) based optically active microdisk resonators. Room temperature photoluminescence from single microdisks shows the characteristic modal structure of whispering-gallery modes (WGM). Highest quality factors of up to 7000 at visible wavelengths, where Si QDs absorb strongly, have been measured for the first time.

Apart from conventional flat and circular resonators, we demonstrate for the first time a new class of active microdisk resonators with out-of-plane bending. In these devices, composed of silicon nitride, Si_3N_4 and Si QD-rich silicon oxide, SiOx, materials, the engineered stress at the interfaces results in bent-up (cup-like) and bent-down (umbrella-like) resonators, depending on which material is used as a top layer. Both type of bent devices support perfectly WGMs and, quite unexpectedly, offer a rich and interesting physics, in particular, the possibility of tuning and enhancing the Q-factor band of WGM modes in bent disks. Generally, the wavelength dispersion of two main different loss-channels, the material absorption and radiative losses, result in a limited bandwidth where the highest Q-factors can be observed (Q-band). We show here, that in a bent resonator, with respect to a flat one (same diameter, thickness and amount of Si3N4 and SiOx materials in both), the maximum of the Q-factor band blue-shifts by more than 70nm (from 832nm to 760nm). In addition, the absolute maximum of Q-band in a bent resonator is 3-4 times higher than that of the flat disk at the wavelength of 760nm. We explain this phenomenon by a smart interplay between the modified dispersions of material absorption and radiative loss related Q-factors (simultaneous increase of Q_{mat} and decrease of Q_{rad}).

Importantly, this tuning scheme does not require larger device sizes, but rather utilizes self-adjustment properties of originally stressed resonator core. Remarkably, the bent resonators benefit from unmodified free-spectral range and cleaner WGM spectra due to the absence of higher order mode families.

Keywords: Whispering-gallery modes, microdisk resonator, Si nanocrystals, emission

1. INTRODUCTION

WGM resonators and Q-factor – High quality monolithic resonators such as micro-disks, rings and toroids are in the focus of an intensive and rapidly evolving research owing to their ability to confine electromagnetic energy in ultrasmall dielectric volumes. In these structures continuous total internal reflection leads to circularly propagating optical modes, called whispering-gallery modes (WGM) [1]. Much interest is focused on two-dimensional whispering-gallery mode (WGM) resonators [2, 3], such as micro-disks [4], rings [5] and toroids [6]; these are chip-integrable and offer a wide spectrum of possible applications ranging from sensing [7] to microdisk lasers [8, 9].

*pucker@fbk.eu; phone 39 0461-314429; fax 39 0461-302040; http://www.fbk.eu

‡ currently at Dept. d'Electrònica, Uni. Barcelona, Barcelona, Spain

Photonic Materials, Devices, and Applications III, edited by Ali Serpengüzel, Gonçal Badenes, Giancarlo C. Righini,
Proc. of SPIE Vol. 7366, 73660M · © 2009 SPIE · CCC code: 0277-786X/09/$18 · doi: 10.1117/12.821603

The main figure of merit of a WGM microresonator is the mode Q-factor, which is a measure of the energy stored in the resonator versus the energy dissipated per round trip. Q-factor engineering is getting relevance since it improves significantly device performance; for example, in optically passive resonators (based on transparent materials with negligible absorption losses), extremely high quality factors ($Q \sim 10^6$ to 10^{10}) can be achieved, offering applications in spectroscopy and sensing [2, 10]. In biosensing applications, for example, utilizing WGM detection schemes, analyte molecules, bound to the resonator surface, spoil cavity Q through light absorption or scattering, thus, an enhanced detection sensitivity benefits from high-Q's at wavelengths of stronger absorption.

On the other hand, in optically active resonator systems, such as III-V semiconductor quantum dot microdisk lasers, the resonator active Q's are usually do not exceed 10^3–10^5 (sufficient, however, for achieving lasing) in the visible and near infrared wavelength range [4, 8, 9, 11]. Nevertheless, Q-engineering (high Q's) for active μ–disks is desirable in spectral windows of maximum material gain; possible resonant mode competition can be overcome with an appropriate tuning of spectral positions of high-Q modes towards the gain band peak, without modifying the free-spectral range (FSR) of resonator modes.

Basic schemes to shift high Q-factors from long to short wavelengths rely on achieving a stronger confinement of WGM modes within the resonator device; this is achieved either by increasing the μ–disk diameter or the thickness, both imposing larger device dimensions. As a consequence, these solutions cause unavoidable reduction of mode FSR and appearance of higher order mode families.

Si nanocrystal-doped active WGM resonators – The recent challenges in silicon photonics towards using nanocrystalline Si as an integrated light source have boosted an intensive research in the last decade [12, 13, 14, 15, 16]. However, as an important cavity system, nc-Si-based microdisk structures have been little studied and only few works appear in the literature [17, 18]. Optically active μ–disk resonators are easily realized by annealing a non stoichiometric SiO_x material (known as silicon-rich silicon oxide, SRO) and, thus, inducing a phase separation of SiO2 and silicon with the formation of Si nanocrystals (Si-nc) [19]. These show strong room-temperature emission in a wide spectral range (700-900 nm) [20], and a smooth increasing absorption band with a threshold at about 800 nm [21].

In this study we present our recent results on WGM emission properties of single microdisk resonators with an optically active disk material made of luminescent nc-Si embedded in SiO_x matrix [22]. We report on subnanometer WGM resonances corresponding to quality factors of few thousands around the wavelength of 800 nm (up to 7000), which to our knowledge are the highest among the previously reported values in nc-Si-based systems. We demonstrate the importance of exciting a single resonator out of the mass-produced microdisk array in order to reveal the fine modal structure in the light emission. Additionally, we show an almost 13-fold narrowing of characteristic linewidths at lowest excitation power associated to an attenuation of excited carrier absorption losses.

Finally, we describe a strategy for tuning and enhancing Q-bands using a new class of micro-resonators, which we refer to as *micro-kylix resonators* [23]. In these devices residual stresses within an initially flat bilayer (silicon nitride, Si_3N_4,and SRO) disk result in either concave or convex devices. To shift the Q-band by 60nm towards short wavelengths in at micro-disks a 50% diameter reduction is required, which causes severe radiative losses suppressing Q's. With a micro-kylix, we achieve similar tuning and even higher Q's by two orders of magnitude smaller diameter modification (0.4%). Consequently, the μ–kylix resonator benefits from unmodified FSR and cleaner WGM spectra due to the absence of higher order mode families. The phenomenon relies on geometry-induced smart interplay between modified dispersions of material absorption and radiative loss-related Q-factors. Such devices can provide new functionalities and novel technological solutions for photonics and micro-resonator physics.

2. SILICON-NANOCRYSTAL MICRODISK RESONATORS

2.1 Experimental details

Sample preparation

Our samples have been produced using standard silicon microfabrication technology (see Figure 1). An SRO layer of 135 nm was deposited on top of crystalline silicon wafers from a mixture of silane (SiH_4, 65 sccm) and nitrous oxide (N_2O, 973 sccm) gases using a parallel-plate plasma enhanced chemical vapor deposition (PECVD) chamber (deposition rate of ~129 nm/min). A successive one hour annealing in an N_2 atmosphere at 1100 °C leads to the formation of Si nanocrystals in the SiO_x host (with ~10% of Si atoms in the nanocrystaline phase) [20]. Then the wafers were

photolithographically patterned and dry etched anisotropically using CHF_3/SF_6 gas chemistry. This way arrays of microdisk structures with diameters ranging from 2μm to 10μm were formed. Isolation of the microdisks from the silicon substrate was realized by an isotropic wet etch of the latter, which formed mushroom-like devices (Figure 2).

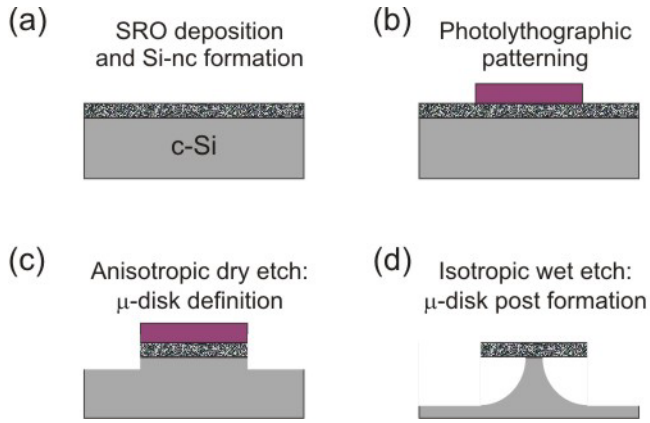

Fig. 1. Fabrication process flow for Si-nc microdisk resonators; (a) PECVD deposition of SRO and formation of Si-ncs through high-temperature annealing, (b) photolithographic patterning of circular structures on top of SRO layer. (c) An anisotropic dry etch step transfers the resist pattern to the SRO layer, and (d) in a successive wet (isotropic) etch forms posts to isolate the microdisk from the Si substrate.

Micro-Photoluminescence measurements

Room temperature micro-PL measurements have been performed using the 488 nm line of an Argon laser (see Fig.3). A long working distance objective was used to focus the laser beam on the samples. The microdisks close to the cleaved sample edge were excited vertically, while the WGM emission was monitored in the plane of disks. The signal was collected through a 25x short working distance objective under small solid angle in the plane of the disks. A polarizer was placed in the collection line to select transverse electrically (TE) or transverse magnetically (TM) polarized PL emission. Finally, the collected signal was sent to a spectrometer interfaced to a cooled silicon charge coupled device (CCD). The PL characterization was performed for microdisk arrays of various diameters, while here, for simplicity, we focus our attention on the discussion of results obtained for the 8μm diameter resonators.

2.2 Discussion of results

Whispering-gallery modes in Si-nc emission

We focused the laser excitation onto an individual microdisk (Fig.3(b)) and recorded the resulting PL emission. In fact, from Fig. 4 one observes immediately the fine WGM structure of the single microdisk. The WGMs manifest as emission lines with subnanometer full width at half maxima (FWHM), leading to quality factors of almost 3×10^3. This Q's are limited by the spectral resolution of our micro-PL setup; in fact, higher precision measurements reveal quality factors of up to 7000 (see the inset of Fig. 4). We note that the trade-off between lower material absorption and weaker confinement of WGM modes at longer wavelengths on one side, and the limited emission band of nanocrystals on the other, result in a limited bandwidth were high Q factors can be observed.

To get some insight on the light confinement inside the microdisk resonator, we have performed effective index mode simulations of a slab waveguide structure with the same thickness (d=135 nm) and material refractive index (1.8 at 800 nm). For such choice of parameters, we have obtained a well confined TE mode (n_{eff} =1.34) while an almost-radiative TM mode (n_{eff} =1.08). These effective refractive indices represent the upper limits for the n_{eff}(TE,TM) of the 3D resonator structure. We, therefore, expect that our microdisk does not support a guided TM mode. This is confirmed both by experimental results (not shown here) and by 3D finite-difference time-domain simulations using a freely available software package [24, 25].

For the TE polarization the simulations predict the existence of two radial families (radial mode numbers p=1,2). However, the measured TE-spectra (Fig. 4) show only the p=1 modes, because the second family is much less intense. Thus, all the observed spectral peaks belong to the same family and for this range of wavelengths the corresponding azimuthal mode numbers extend from m=29 (928 nm) to m=42 (710.5 nm), with an average mode spacing of FSR~15 nm.

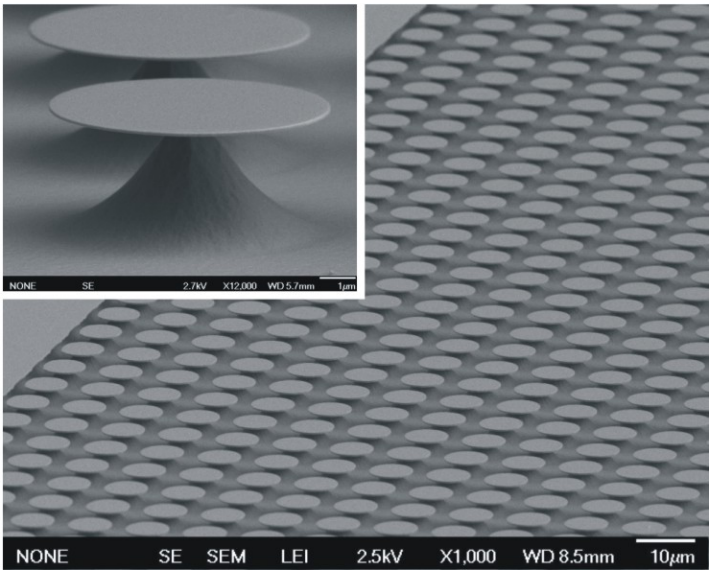

Fig. 2. Scanning electron micrographs of microdisk arrays and a single device (inset).

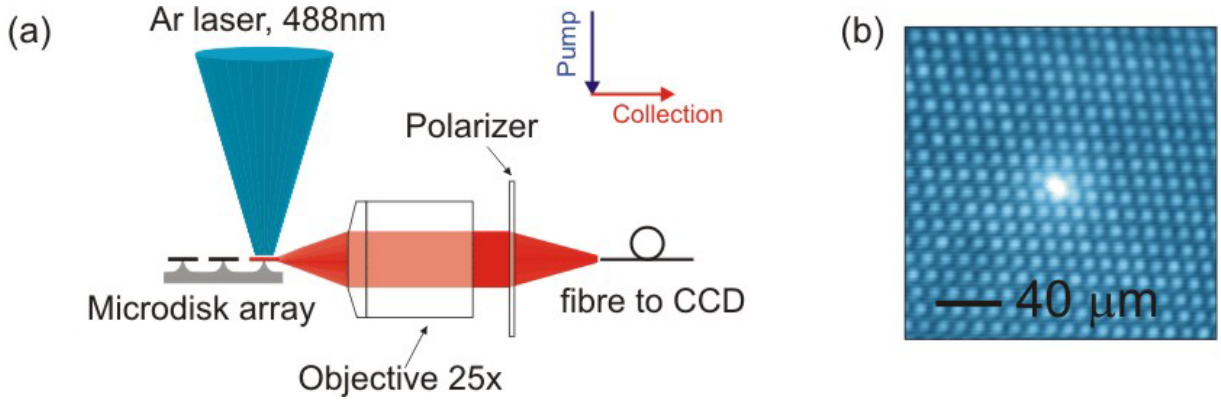

Fig. 3. (a) The micro-PL setup; individual microdisks are excited vertically through a focused pumped beam (CW Argon laser, 488nm), while the characteristic WGM emission is collected through a 25x short working distance objective under small solid angle in the plane of the disks. The polarization of the collected signal is further selected by a polarizer and sent to a cooled Si charge coupled device. (b) The bright spot in the photograph is the direct image of the visible PL emission of nc-Si from a single disk resonator.

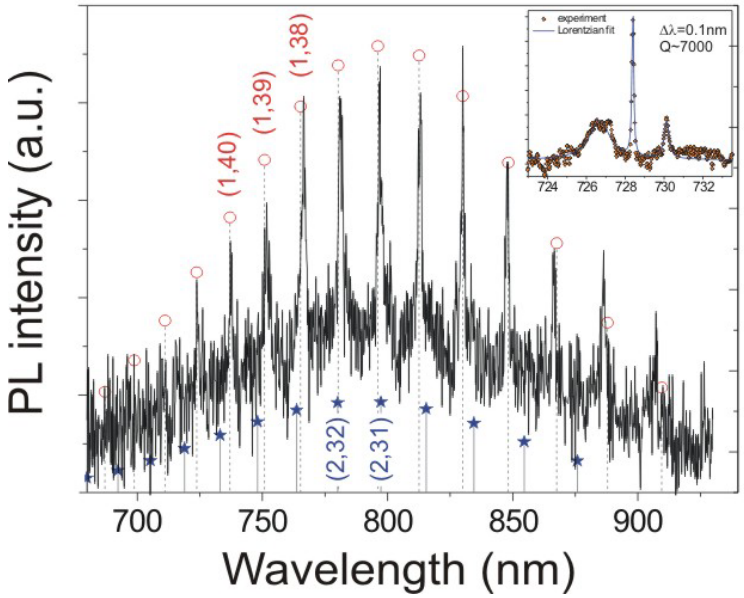

Fig. 4. Measured TE-polarized WGM spectrum of an 8μm diameter microdisk is plotted together with the simulated peak positions for the first radial mode family (empty circles). The predicted second mode family (full stars) is however absent in the measured spectrum because of being much less intense. The inset shows a high-resolution spectrum of first family mode (central peak) with a quality factor of ~7000.

Pump power induced mode broadening due to Excited Carrier Absorption

Finally, we address some issues related to the influence of pumping power on the WGM characteristics of our microdisks, in particular, the observed significant linewidth modification. In Fig. 5(a) we report the measured Q's of few distinct resonances at λ =754 nm, 768 nm and 849 nm (m =39, 38 and 33, respectively) of thin microdisks. A monotonic, roughly 13-fold attenuation of Q factors as the pump power increases from 1.25 to 100 mW.

Attenuating Q factors suggest that at higher excitation powers we either introduce an additional loss source or enhance the existing ones. In a microdisk resonator, the total loss, resulting from different loss mechanisms, is expressed through the sum of inverse of possible limiting Q factors:

$$Q^{-1} = Q_{rad}^{-1} + Q_{mat}^{-1} + Q_{ssc}^{-1} + Q_{sa}^{-1}, \quad (1)$$

where the inverse of Q_{rad}, Q_{mat}, Q_{ssc} and Q_{sa} correspond to radiation, material (bulk absorption and propagation), surface scattering and surface absorption losses, respectively. Last two terms, in our case, can be considered independent on the pump power within a good approximation.

Thus, possible modifications of Q can arise from power-modified Q_{rad} and Q_{mat}. Being related to the disk geometry, the radiative Q can be considered independent of pump power, since no spectral shift of WGM modes or changes in FSR are observed between lowest and highest powers (i.e., no disk size modification due to thermal heating or material index changes).

The material Q-factor is defined as $Q_{mat} = 2\pi\, n_g /(\lambda\alpha)$, with n_g ($\approx n_{eff}$) being the group index and α - the material loss coefficient. In recent studies on nc-Si containing waveguide systems, pump power induced losses at 1.5μm wavelength have been addressed and attributed to excited carrier absorption (ECA) [26, 27]. We believe that the same mechanism occurs here; Si nanocrystals absorb strongly at visible wavelengths creating an exciton. Part of the excitons can successively absorb other photons to promote electrons to higher energetic levels in the nanocrystal conduction band.

Such absorption events will enhance the cavity losses, causing the observed WGM broadening. While under low pump conditions the ECA loss is expected to increase linearly with power, P, at high pump powers different phenomena can deviate this simple relationship; a number of processes, such as the ECA itself (re-absorption of either a pump or emitted photon by an already formed exciton), Auger recombination and the saturation of the number of excitable nanocrystals will induce additional non-linear N(P) behavior. This non-linearity is clearly observable in all our experimental data (Fig.5(a)). Assuming a power-dependent loss, $\alpha = \alpha_0 + \alpha^*(P)$, one can rewrite Eq. 1 as

$$Q_{exp}^{-1}(P) = \left(\sum Q_{rad,ss,sa}^{-1} + \frac{\lambda \alpha_0}{2\pi n_{eff}} \right) + \frac{\lambda \alpha^*(P)}{2\pi n_{eff}}. \qquad (2)$$

Here α_0 stands for the material passive loss coefficient, which has been independently estimated from ellipsometric data and at λ = 754 nm is of the order of 30 cm^{-1} or less [28]. The first two terms on the right part of Eq. 2 represent the inverse of Q of the passive microdisk and, as mentioned above, can be considered as a constant term. With this, for the measured data $Q_{exp}^{-1}(P)$ a non-linear fitting function in the form $\alpha^*(P)=xP/(1+yP)$, based on the rate equation model [27], has been applied (Fig. 5(b)).

The quality of the fit is further confirmed through the following procedure. We consider the fitting value for the passive Q (the constant term in Eq. 2), the FDTD-simulated geometrical quality factor $Q_{rad} \approx 1.1\times10^4$ for 8 μm disks and negligible surface scattering/surface absorption losses, and back-calculate the material passive loss coefficient. Such obtained $\alpha_0 \approx 32$ cm^{-1} is in very good agreement with the ellipsometric results.

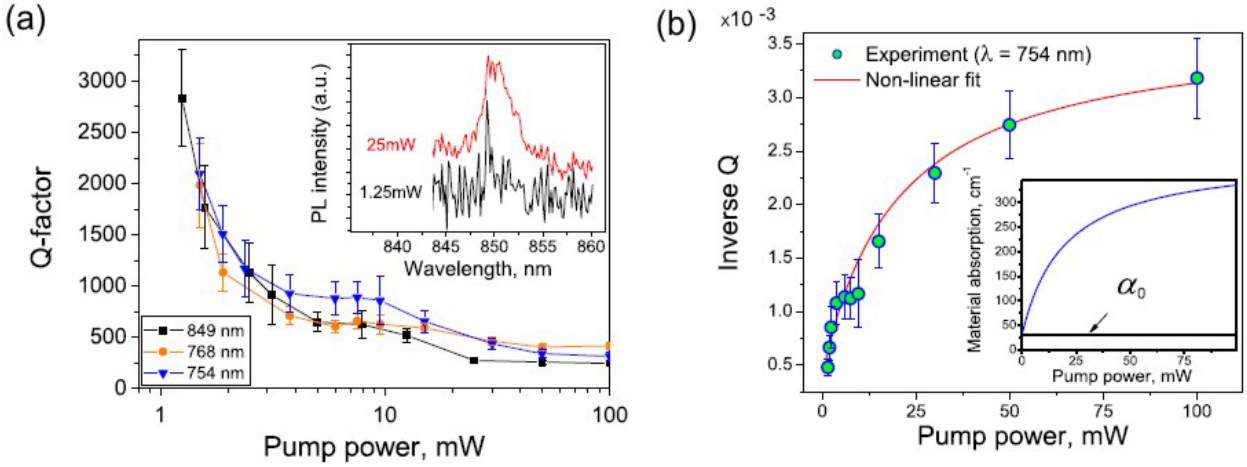

Fig. 5. Pump induced excited carrier absorption in Si-ncs and modification of WGM Q-factors: (a) The measured Q-factors at increasing pump power are plotted at three different wavelengths, reporting an order of magnitude variation between two extreme pump powers (error bars reflect the accuracy limit of measured linewidths). The inset shows the WGM mode at λ = 849 nm at the lowest and at a high pump powers. (b) Non-linear fit of the measured inverse Q_{exp} at λ = 754 nm (m =39) using Eq. 2. The inset shows the corresponding power-dependent absorption coefficient $\alpha = \alpha_0 + \alpha^*(P)$.

We stress that ECA will figure as the main limiting factor for a possible multi-wavelength lasing from the nc-Si-based microdisk. The SRO material optimization (low-loss, positive material gain) should play a key role for further enhancement of the observed Q-factors of few thousands.

To conclude, in this first part of our study we reported on PL emission properties of individual, optically active microdisk resonators with Si nanocrystals. We observed subnanometer whispering-gallery resonances in visible light emission with quality factors in excess of 7000 from single microdisk resonators. Moreover, the influence of pumping power on the WGM narrowing has been addressed, showing more than an order of magnitude enhancement of Q-factors

due to an attenuation of pump-induced loss mechanisms. Both qualitative and quantitative analysis suggest that the excited carrier absorption stands behind the observed phenomenon.

3. SILICON-NC MICRO-KYLIX RESONATORS FOR Q-BAND TUNING

In this section we report on a new class of μ–disk resonators, which we call micro-kylix (μ–kylix) resonators (Fig. 6(a)), in analogy with the Greek wine-drinking cup - *κυλιξ*, (inset photo, Fig. 6(a)) [29]. These present a bent μ–disk con_guration, which, owing to an appropriate stress-engineering approach, can be realized both as a bent-up (cup-like, μ–kylix) or bent-down (umbrella-like, inverse μ–kylix) resonators. These devices support perfectly whispering-gallery modes and, at the same time, posses new and unexpected physical characteristics. The most striking of these, perhaps, is that their geometry induces a tuning of the Q-factor band of resonator modes towards the stronger material absorption range without degrading highest Q's. Importantly, this tuning scheme does not require larger device sizes, but rather utilizes self-adjustment properties of originally stressed resonator core. Remarkably, the μ–kylix resonator benefits from unmodified FSR and cleaner WGM spectra due to the absence of higher order mode families.

Numerical results

We used the FDTD tool to check if a m-kylix acts as WGM resonator. Starting with a 10 mm diameter at micro-resonator, we first verified that it supports WGMs, and, then, in a next step, we applied a bending to the at disk in the z-direction (Fig. 6(b)), defining geometrically the bends as

$$(x, y) = (r_{curv} \pm d/2) \sin\left(\frac{\pi}{180}\alpha\right),$$
$$z = (r_{curv} \pm d/2)\left(1 - \cos\left(\frac{\pi}{180}\alpha\right)\right),$$

where $r_{curv}=(L^2+h^2)/(2h^2)$ is the radius of curvature of the disk in the z-direction (see Fig.6(b)) and d is the disk thickness.

Indeed, the numerical simulation confirmed that the μ–kylix supports guided modes. As an example, Fig. 6(c) shows the electrical field distribution of a TM-polarized mode (azimuthal mode number m = 47, λ = 829 nm) close to the edge of the μ–kylix resonator.

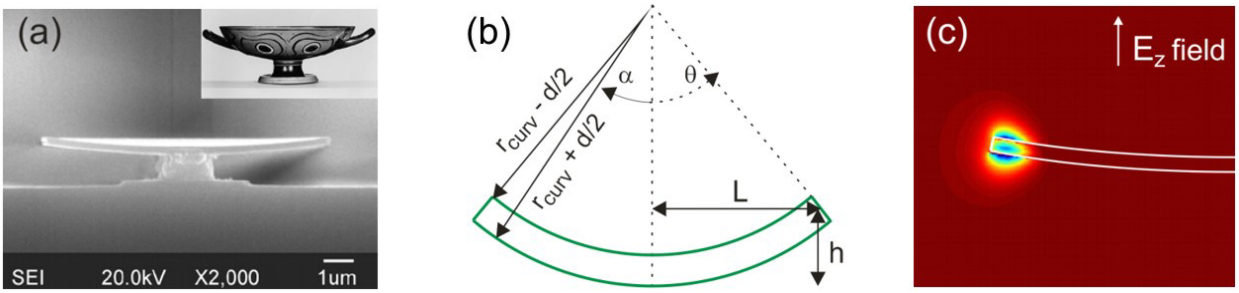

Fig. 6. The micro-kylix resonator. (a) Cross-sectional scanning electron micrograph (SEM) of a micro-kylix resonator. Inset: The Greek wine-drinking cup - *κυλιξ*, with a broad relatively shallow body raised on a stem from a foot [29]. (b) Geometrical sketch explaining the definition of disk bending. (c) Electrical field distribution of the TM-polarized whispering-gallery mode shows a rather good confinement within the core of the μ–kylix resonator.

3.1 Experimental details

Sample preparation

To realize the μ–kylix we used a combination of two materials, silicon-rich silicon oxide SiO_x (SRO) and silicon nitride Si_3N_4. We take advantage of the fact that these two materials posses different thermal expansion coefficients, which lead to unavoidable stresses at the end of the deposition process. The stress can be engineered by accurate control of the deposition temperature and the layer thickness. After disk definition and post formation to isolate the disk from the substrate, the accumulated stress gradients through the layer interfaces bend the micro-disk device Fig. 7. For μ–kylix we first deposit a 160 nm-thick PECVD SiO_x layer on top of crystalline silicon wafers. After the high-T treatment the SRO layer densifies down to 110 nm due to the release of hydrogen and micro-voids, present in the as-deposited layer. The residual compressive stress on SRO/bulk-Si interface was measured to be -100 MPa. In a next step, a similarly thick Si_3N_4 layer was deposited at 780 °*C* using a low pressure chemical vapor deposition (LPCVD) technique (1.25 GPa tensile stress). A photolithographical patterning of disk arrays was followed by dry (anisotropic, disk formation) and wet etching (isotropic, post formation) steps.

In this way, μ–kylixes are obtained by engineering the stress in the bilayer structure (Fig. 6(a)). Such a technological solution is quite simple (common) and, in addition, is combined to a large degree of freedom for not only the choice of materials, but also control of both the degree and the direction of disk reshaping. For example, the bending degree (the out-of-plane lifting of the disk edge) is strictly related to the thickness ratio of the two different materials, while the direction of bend (cup or umbrella) can be easily changed inverting the materials (Fig.7(e) and (f), respectively).

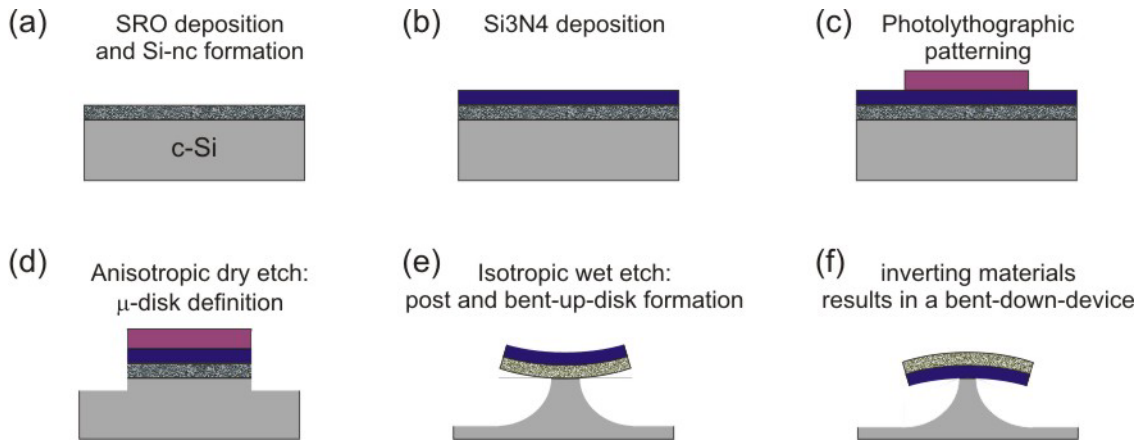

Fig. 7. The micro-PL setup; individual microdisks are excited vertically through a focused pumped beam (CW Argon laser, 488nm), while the characteristic WGM emission is collected through a 25x short working distance objective under small solid angle in the plane of the disks. The polarization of the collected signal is further selected by a polarizer and sent to a cooled Si charge coupled device.

Micro-Photoluminescence measurements

We measured the room-temperature micro-photoluminescence emission from single resonators in a free-space collection configuration, described above (see Fig. 3)). We observed sharp, sub-nanometer modal peaks raising out from the wide emission band of Si-nc due to WGM. The measured spectrum (Fig. 8(a)), at first glance, is qualitatively similar to that observed from single-layer-SRO μ–disks (Fig. 4), with the difference that the narrowest resonances here manifest at shorter wavelengths (see Fig. 8(a), down triangles).

In order to confirm it quantitatively, we prepared a flat μ–disk, consisting of the same amount of SRO and Si_3N_4 as in a μ–kylix resonator. In order to have the disk at, we sandwiched the SRO layer between two 55 nm-thick Si_3N_4 layers (this

guarantees a total thickness and weighted-average refractive index of the μ–disk similar to those of the μ–kylix). We measured the WGM emission spectrum of the μ–disk (Fig. 8(b)) and compared with that of the μ–kylix. The performed Lorentzian fit analysis of all appreciable peaks, plotted in Figure 3(d), evidences an important modification of Q-factors in μ–kylix. We observe that the Q-band maximum in the μ–kylix is blue-shifted by almost 60 nm with respect to that of the μ–disk. As a consequence, this shift results in higher Q-factors (roughly four-fold) at wavelengths (~ 760 nm), where our active material, SRO, has stronger absorption.

Discussion

In few micron-sized resonators, the total Q-factor dispersion is defined mainly by the interplay between the radiative and material Q's, expressed as

$$Q_{total}^{-1}(\lambda) \approx Q_{rad}^{-1}(\lambda) + Q_{mat}^{-1}(\lambda) + Q_{i}^{-1}, \tag{3}$$

with the semi-empirical term Q_i accounting for losses due to non-idealities in real devices. Moreover, in active micro-resonators the measured Q-band of WGM emission is limited to the spectral region of the active material luminescence band, in our case, that of Si-nc.

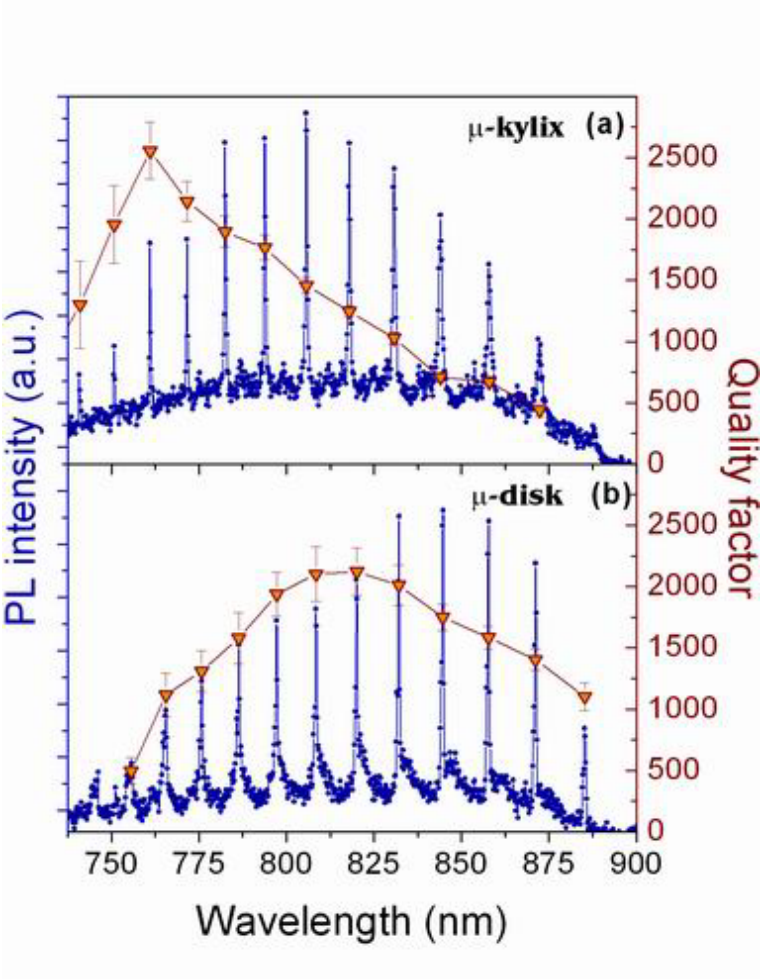

Fig. 8. The WGM spectra (—●—) and corresponding Q-factors (—▼—) of (a) a μ–kylix resonator and (b) a flat conventional disk. The Q-band maximum in the μ–kylix is blue-shifted by almost 60 nm with respect to that of the flat disk.

The possibility of having modified radiative losses in our bent devices is rather straightforward. This can be expected, since the stress-induced formation of μ–kylix resonators (from nominally 10 μm at disks), reduces slightly the disk external diameter (by ~ 50 nm). In the case of flat conventional μ–disks, such a small modification of the diameter (by 0.4% only), is not expected to affect significantly the radiative losses (Q_{rad}^{-1}). For example, for 200 nm-thick passive devices of 10 μm and 9.96 μm of diameter (both flat), the typical values of radiative Q at a wavelength of λ = 800 nm are of the order of 10^6, differing by ~5% only (see Fig. 9(a), ● and ▲).

On the contrary to this, our numerical simulations show that in a μ–kylix resonator of 9.96 μm diameter Q_{rad} reduces by an order of magnitude with respect to the original μ–disk (Fig. 9(a), ▼). This tenfold reduction in radiative Q associated to disk reshaping is an interesting result which has never been addressed. To model this, we introduce the concept of out-of-plane bending loss ($1/Q_{bend}(z)$), which is a function of the bending degree, i.e. of the coordinate z of the out-of-plain lifting of the disk edge. With this, one can model the radiative Q for a μ–kylix resonator as

$$Q_{rad}^{-1}(R,z) = Q_{rad}^{-1}(R) + Q_{bend}^{-1}(z), \tag{4}$$

with $Q_{rad}(R)$ standing for the radiative Q-factor for a flat resonator of radius R. Our FDTD calculations show that most of the reduction of Q_{rad} are due to the bending quality factor Q_{bend}. This change in Q_{rad} leads to an important spectral blue-shift of the Q-band, with, however, an overall reduction of Q values. Not observing this in our experiments, we conclude that in μ–kylix resonator the Q_{mat} is also increased (this scenario is not easily predictable).

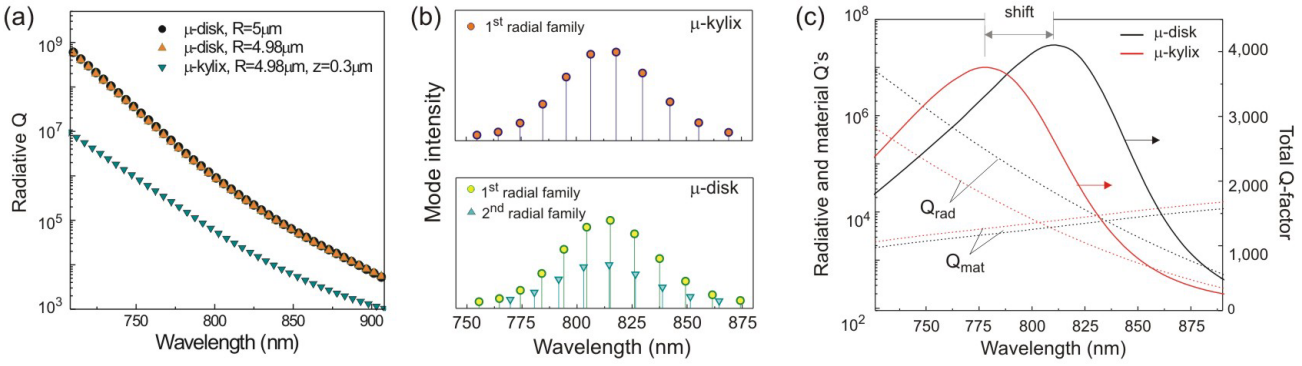

Fig. 9. The WGM spectra (—●—) and corresponding Q-factors (—▼—) of (a) a μ–kylix resonator and (b) a flat conventional disk. The Q-band maximum in the μ–kylix is blue-shifted by almost 60 nm with respect to that of the flat disk.

Our further analysis suggest that possible modifications in Q_{mat} , should result from differences in group indices and/or confinement factors, Γ. We reveal very similar n_g for both μ–disk and μ–kylix (n_g ≈2.02 and 2.12 at 800 nm, respectively). In contrast to slab-waveguide simulations for various layer sequences, showing almost identical Γ's, we observe important differences in a microdisk geometry. In particular, the μ–kylix shows smaller Γ's than the μ–disk (Γ ≈0.31 and 0.4 at 800 nm, respectively). Since Q_{mat} is inversely proportional to Γ, this roughly 25% less confinement leads to an important change in material Q's. This last, in its turn, modifies the Q-band, shifting it further to shorter wavelengths, but, more importantly, does not degrade highest Q values. In addition, from this analysis it is possible to explain why the μ–kylix resonators do not support higher order mode families (Fig.8(a)), on the contrary to μ–disks (Fig.8(b), see the broadened and damped peaks next to sharp first order families); the overall reduced confinement in μ–kylix alters guided mode propagation for higher order families. This is confirmed through numerical calculations shown in Fig. 9(b). Combining our numerical results for both modifications in Q_{rad} and Q_{mat} , it is possible to reproduce qualitatively the experimentally observed Q-band tuning (Fig. 9(c)).

It is important to note, that in conventional μ-disk resonators smaller diameters blue-shift the spectral range of highest Q-factors too. For example, a 60 nm shift of the Q-band is observed for μ-disk of twice smaller diameter (Fig. 10). In this case, the only modification in Q_{total} arises from a severe attenuation of Q_{rad}'s, therefore, very low values of highest Q_{total} are observed. Moreover, the free spectral range in a 5 μm μ-disk doubles with respect to a 10 μm one. We underline, that the μ-kylix configuration provides the same amount of tuning of the Q-band with only a 0.4% of effective diameter modification, which also provides an almost unmodified FSR.

Concluding this section, we have demonstrated a new class of bi-dimensional micro-resonators with out-of-plane bending, which perfectly support whispering-gallery modes. We refer to them as micro-kylixes. This resonators are chip-integrable and can be easily fabricated using standard microfabrication technology. Their particular geometry reveals new physics: tuning of the highest Q-factors towards shorter wavelengths, where the basic material has stronger absorption. This is achieved through a smart interplay between radiative and material quality factors. Our experimental results, validated by numerical simulations, indicate that this physical phenomenon could be exploited to obtain improved Q-factors in specific spectral windows (shorter wavelength) without modifying resonator's physical size and the free spectral range. Micro-kylix resonators can offer novel technological solutions for micro-resonator physics and photonics research and may open the door to new functionalities of resonator devices, from sensing to optical amplification.

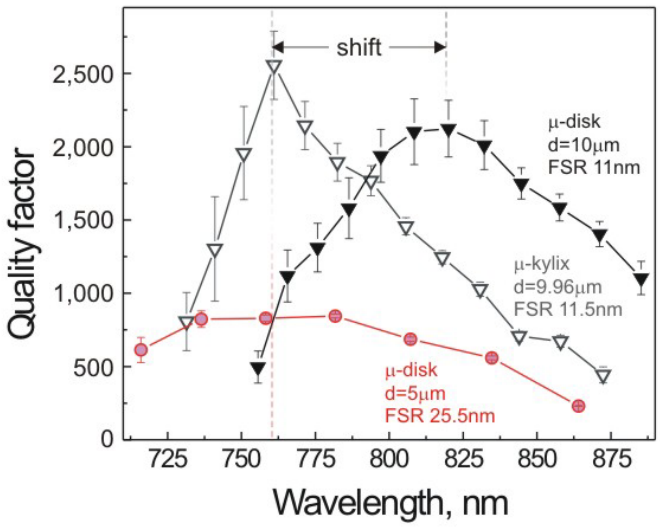

Fig. 10. Q-band shift in smaller flat disks: a 60 nm spectral shift of the Q-band is measured for twice smaller (5 μm) μ-disks, while the same shift can be achieved with a μ-kylix of only 0.4% smaller effective diameter.

ACKNOWLEDGEMENTS

The authors would like to thank a number of collegues, P. Bettotti, M. Xie, I. Carusotto, P. Belluti, A. Picciotto, E. Sera, B. Margesin and F. Giacomozzi for their support and stimulating discussions.

REFERENCES

[1] L. Rayleigh, Philos. Mag. **27**, 100 (1914).
[2] A.B. Matsko, and V.S. Ilchenko, IEEE J. Sel. Topics Quantum Electron. **12**, 3 (2006).

[3] K.J. Vahala, Nature (London) **424**, 839 (2003).
[4] S.L. McCall, A.F.J. Levi, R.E. Slusher, S.J. Pearton, and R.A. Logan, Appl. Phys. Lett. **60**, 289 (1992).
[5] T. Krauss, P.J.R. Laybourn, and J. Roberts, Electron. Lett. **26**, 2095 (1990).
[6] D.K. Armani, T.J. Kippenberg, S.M. Spillane, and K.J. Vahala, Nature **421**, 925 (2003).
[7] A.M. Armani, and K.J. Vahala Opt. Lett. **31**, 1896 (2006).
[8] P. Michler, A. Kiraz, L. Zhang, C. Becher, E. Hu, and A. Imamoglu, Appl. Phys. Lett. **77**, 184 (2000).
[9] Zh. Zhang, L. Yang, V. Liu, T. Hong, K. Vahala, and A. Scherer, Appl. Phys. Lett. **90**, 111119 (2007).
[10] A.M. Armani, D.K. Armani, B.Min, K.J. Vahala, and S.M. Spillane, Appl. Phys. Lett. **87**, 151118 (2005).
[11] K. Srinivasan, A. Stintz, S. Krishna, and O. Painter, Phys. Rev. B **72**, 205318 (2005).
[12] L. Pavesi, L. Dal Negro, C. Mazzoleni, G. Franzo, and F. Priolo, Nature (London) **408**, 440 (2000).
[13] *Towards the First Silicon Laser*, NATO Science Series, edited by L. Pavesi, S. Gaponenko, and L. Dal Negro (Kluwer, Dordrecht, 2003).
[14] A.S. Liu et al., Nature (London) **427**, 615 (2004).
[15] H. Rong et al., Nature (London) **433**, 292 (2005).
[16] Q.F. Xu, B. Schmidt, S. Pradhan, and M. Lipson, Nature (London) **435**, 325 (2005).
[17] R.-J. Zhang, S.-Y. Seo, A.P. Milenin, M. Zacharias, and U. Gösele, Appl. Phys. Lett. **88**, 153120 (2006).
[18] R.D. Kekatpure and M.L. Brongersma, Phys. Rev. A **78**, 023829 (2008).
[19] L. Pavesi and D. Lockwood, *Silicon Photonics*. Topics in Applied Physics vol. **94** (Springer-Verlag, Berlin, 2004).
[20] L. Ferraioli, M. Wang, G. Puker, D. Navarro-Urrios, N. Daldosso, C. Kompocholis, and L. Pavesi, J. Nanomaterials 2007, 43491 (2007).
[21] G.V. Prakash, M. Cazzanelli, Z. Gaburro, L. Pavesi, F. Iacona, G. Franzò, and F. Priolo, J. Mod. Opt. **49**, 719 (2002).
[22] M. Ghulinyan, D. Navarro-Urrios, A. Pitanti, A. Lui, G. Pucker and L. Pavesi, Opt. Express **16**, 13218 (2008).
[23] M. Ghulinyan, A. Pitanti, G. Pucker and L. Pavesi, submitted (2009); arXiv:0903.3829v1.
[24] A. Farjadpour, R. Roundy, A. Rodriguez, M. Ibanescu, P. Bermel, J.D. Joannopoulos, S.G. Johnson, and G. Burr, Oppt. Letters **31**, 2972 (2006).
[25] V.A. Mandelshtam, and H.S. Taylor, J. Chem. Phys. **107**, 6756 (1997); erratum, ibid. **109**, 4128 (1998).
[26] D. Navarro-Urrios et al., Appl. Phys. Lett. **92**, 051101 (2008).
[27] R.G. Elliman, M. Forcales, A.R. Wilkinson, N.J. Smith, Nucl. Instrum. Meth. Phys. Res. B **257**, 11 (2007).
[28] The quality of fit to ellipsometric data saturates down to values $\chi^2 \sim 0.1$ for loss coefficients smaller than $\alpha 0=30 cm^{-1}$.
[29] image source http://it.wikipedia.org/wiki/Kylix